Accepted Manuscript

Spin-dependent electrochemistry: Enantio-selectivity driven by chiral-induced spin selectivity effect

Mirko Gazzotti, Serena Arnaboldi, Sara Grecchi, Roberto Giovanardi, Maria Cannio, Luca Pasquali, Agnese Giacomino, Ornella Abollino, Claudio Fontanesi

Please cite this article as: M. Gazzotti, S. Arnaboldi, S. Grecchi, R. Giovanardi, M. Cannio, L. Pasquali, A. Giacomino, O. Abollino, C. Fontanesi, Spin-dependent electrochemistry: Enantio-selectivity driven by chiral-induced spin selectivity effect, *Electrochimica Acta* (2018), doi: 10.1016/j.electacta.2018.08.023.

Spin-Dependent Electrochemistry:

enantio-selectivity driven by chiral-induced spin selectivity effect.

Mirko Gazzotti[1], Serena Arnaboldi[2], Sara Grecchi[2], Roberto Giovanardi[1], Maria Cannio[1], Luca Pasquali[1,#,$], Agnese Giacomino[3], Ornella Abollino[4], Claudio Fontanesi[1]*

[1]Department of Engineering 'Enzo Ferrari', University of Modena and Reggio Emilia, Via Vivarelli 10, 41125 Modena, Italy

[2]Department of Chemistry, University of Milan, Via Golgi 19, 20133 Milano, Italy

[3] Department of Drug Science and Technology, University of Torino, Via Giuria 9, 10125 Torino, Italy

[4] Department of Chemistry, University of Torino, Via Giuria 5, 10125 Torino, Italy

[#]IOM-CNR, s.s. 14, Km. 163.5 in AREA Science Park, 34149 Basovizza, Trieste, Italy

[$]Department of Physics, University of Johannesburg, P.O. Box 524, Auckland Park 2006, South Africa

Abstract

Spin-Dependent Electrochemistry (SDE) is a new paradigm in electrochemistry where the electrochemical response of a chiral electrode|solution interface is studied as a function of spin-polarized current. In this work, the SDE concept is further developed exploring the use of the "chiral imprinting" concept, which is implemented in two different, complementary, ways i) a chiral compound in bulk solution to obtain chiral-induced spin selectivity effect at the ferromagnetic (FM) electrode surface ii) conversely, a chiral-ferromagnetic (CFM) hybrid working electrode is produced: nickel is electrochemically co-deposited with a chiral compound, L-ta or D-(−)-tartaric acid, which is added to the electrodeposition bath; this allows to obtain a chiral co-deposited nickel-tartaric acid (Ni-LTA or Ni-DTA) working electrode. As a further innovation, the ferromagnetic working electrode is prepared by direct Ni electrodeposition on the north, or south, pole of a permanent magnet. The electrochemical response of these two chiral imprinted systems is studied by comparing cyclic voltammetry (CV) curves. The latter are recorded in the potential range relevant to the Ni(III)/Ni(II) electrochemical equilibrium, and also in the presence of glucose in bulk solution. An impressive variation in peak potentials is found when comparing CVs recorded on the north, versus south, pole of the magnet (in particular, when the co-deposited CFM working electrode is used). These results are properly rationalized within the Chiral-Induced Spin Selectivity (CISS) effect.

* corresponding author e-mail address: claudio.fontanesi@unimore.it

1. Introduction

Charge transport in chiral systems, through chiral interfaces, is *per se* a fascinating subject [1]. Indeed the interplay between charge transmission, chirality and magnetism is a field of fundamental science yet open to discussion. Moreover, besides its intrinsically intriguing aspects, a number of practical applications are here involved. For instance, enantio-recognition is one fundamental aspect of the yet unfolded problem of homochirality in nature, i.e. the fact that the majority of chiral natural compounds is right handed, a major fundamental problem in nature still open to discussion [2,3]. In the field of electrochemistry enantio-selective molecular architectures are quite often obtained by the preparation of high quality surfaces to be used as electrodes, where chiral surfaces are obtained exploiting a number of different methodologies: adsorption of chiral organic compounds [4–6], chiral imprinted electrode surfaces using for instance tartaric acid or chiral liquid crystals [7–10], chiral metal surfaces obtained by application of a rotating high-intensity magnetic field [11–13]. The concept of chiral-imprinted systems has been pushed further as recently demonstrated in some papers by Mussini and Sannicolò where the presence in bulk solution of chiral compounds was used to "induce" enantio-selectivity, or generate local spatial chirality effects: for instance in cyclic voltammetry experiments carried out in chiral ionic liquids, as well as in achiral ionic liquids where chirality is induced by the presence of suitable bulk chiral compounds [14,15]. Within this field, a strongly related area of fundamental research deals with the combination of chiral effect with spin charge transfer properties as in the spin-dependent electrochemistry (SDE) method. The latter is a quite recently proposed paradigm in electrochemistry [16–19]. The peculiar characteristic of SDE is that it allows for the control, production and measurement of spin polarization currents within an electrochemical system. This gives the opportunity to gain further physical insight, and extend the range of possible applications, of the chiral-induced spin-selectivity (CISS) effect [20,21], also allowing to investigate the influence and role of spin in the charge transport and on surface adsorption phenomena when chiral systems are involved [20,22–24]. Further, a possible application of SDE is to enhance the efficiency of the hydrogen production *via* electrochemical dissociation of water: this process is commonly addressed as water splitting (WS) [25–28].

In this work the CISS effect is exploited using the presence of chiral compounds in bulk systems, rather than adsorbed on the electrode surface. Thus, allowing for the achievement of spin polarized currents using a simple and low-cost methodology.

Within this picture, here we present electrochemical evidence which demonstrates that Ni and Ni-chiral electrodes directly supported on a permanent magnet can be exploited as effective spin injectors.

1.1 Spin-dependent electrochemistry/Chiral-induced spin-selectivity

In general, ferromagnetic materials and magnetism are considered as a macroscopic manifestation of the electron spin. Spin-related properties are in general controlled by suitable application of a magnetic field. Within this picture, the CISS effect plays a peculiar role, in that the "spin transport/spin injection" properties are controlled and manipulated by suitable selection of a chiral system [20,21,29]. Implementation of the CISS effect in electrochemistry led to the development of the so-called Spin-Dependent Electrochemistry [16,18,19]. As often the case, in spintronics, spin injection is obtained exploiting the effect of magnetic field on ferromagnetic materials; this at variance of results obtained in quite recent magnetless Hall device based SDE experiments [30]. Figure 1 shows the physics underlying the process of spin injection in a ferromagnetic material.
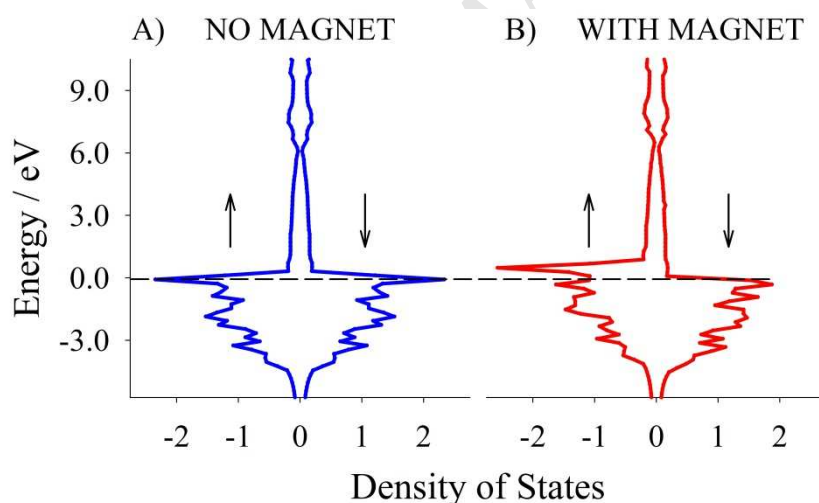

Figure 1. Energy vs Density of States (DOS) pattern, spin polarized theoretical calculation for a Ni fcc crystal: A) without (blue curves) and B) with (red curves) application of a magnetic field. The horizontal dashed line is the Fermi energy. Spin polarized plane wave based calculations [31].

The application of the CISS effect in SDE aims to gain control of spin driven chemical reactivity: allowing for spin control over the Ni oxidation process using two new concepts for the fabrication of the working electrode **i)** magnetic field Ni spin injection in the presence of a chiral compound in bulk solution with a nickel electrode directly electrodeposited (about 10 μm thickness, compare the Supporting Information on the

detailed characterization of the electrodeposited Ni) on the north and south side of a permanent magnet **ii)** a totally new concept, where the electrochemical co-deposition of Ni and L-ta is used to obtain a chiral ferromagnetic working electrode able to enhance spin injection selectivity.

1.2 Electrochemistry oxidation of Ni

The electrochemical oxidation of Ni in alkaline solution is a thoroughly studied process, this because of its use in the field of surface functionalized materials used in the field batteries, sensoristic and electrocatalytic applications [6,32–42]. In alkaline solution nickel is spontaneously covered by a thin film of $Ni(OH)_2$, and the situation is further complicated by existence of a variety of hydrated $Ni(OH)_2$ crystal structures $\alpha - Ni(OH)_2$ and $\beta - Ni(OH)_2$, hydration plays also a role leading to a rather complex picture, which is characterized by a non-stoichiometric behaviour: $Ni(H_2O)_x(OH)_2$ with $0.1 \leq x \leq 0.4$. Upon electrochemical oxidation nickel oxyhydroxide species are formed: $\beta - NiOOH$ and $\gamma - NiOOH$ crystal structures [43]. Indeed, the hypothesis about the presence and distribution of $Ni(OH)_2$ in the film is controversial; in particular Visscher and Barendrecht showed that a first layer of NiO is covered after the positive scan with a thick film of $\beta - Ni(OH)_2$ which is the base material for the practical application in batteries [44]. It must be mentioned that the electrode pre-treatment influences the separation of the oxidation reduction peak potentials, to the electrode pre-treatment [45]. The main reactions and chemical species underlying the appearance of the redox peaks in CVs run in alkaline solutions in the 0 to 0.8 V potential range are shown in reactions (1) to (4) [32,36,46,47]:

$Ni + 2(OH)^- \rightarrow Ni(OH)_2 + 2e^-$	(1)
$Ni(OH)_2 \rightarrow NiOOH + H_2O + 2e^-$	(2)
$Ni(OH)_2 \rightarrow NiOOH + H^+ + e^-$	(3)
$2Ni(OH)_2 \cdot xH_2O \rightarrow [Ni_2(OH)_5 \cdot (x-1)H_2O] + H^+ + e^-$	(4)

2. Experimental

2.1 Chemicals

L-(+)-tartaric acid (L-ta), D-(−)-tartaric acid (D-ta), L-(−)-glucose (L-glu), D-(+)-glucose (D-glu) enantiomers were purchased from Sigma Aldrich and used without further purifications. The nickel electrodeposition was carried out using a Watt's bath:

150 g/L of nickel sulphate, 60 g/L nickel chloride, 37 g/L boric acid, pH = 5. A chiral imprinted ferromagnetic electrode, CFM, is obtained by addition of 0.1 M L-(+)-tartaric acid (or D-(−)-tartaric acid) to the Watt's bath composition: the relevant Ni-LTA or Ni-DTA CFM electrodes are obtained.

2.2 Electrochemical set-up

The electrodeposition was carried out under potentiostatic regime at -1.4 V, 900 seconds total electrodeposition time. The relevant chronoamperometric curves, for the north and south sides of the magnet, are shown in Figure 3SI and 4SI of the Supporting Information. Electrochemical measurements were performed using both Autolab PGSTAT 128N and CHI660A potentiostats, employing a typical three-electrode electrochemical cell. A peculiar arrangement was adopted in the case of Ni electrodeposited on the magnet: a teflon cell, featuring a hole (0.8 cm diameter) in the bottom, was used in a vertical configuration where the Ni-on-the-magnet working electrode was tightened from below, a teflon ring was used to ensure no solution leakage from the cell. Thus, Ni-on-the-magnet surfaces were used as working electrodes, while a Pt sheet and a silver, silver chloride, KCl saturated solution (Ag/AgCl/KCl$_{sat}$) electrodes were the counter (CE) and reference electrodes (RE), respectively. Control experiments, to check the quality of the nickel surface obtained *via* electrodeposition on the magnet, were carried out using glassy carbon, Pt and evaporated gold as working electrodes (compare the Supporting Information). A 0.1 M KOH aqueous solution was used as base electrolyte in all reported electrochemical measurements. A neodymium permanent magnet was used as the substrate for the nickel electrodeposition made on the north (or south) pole. Due to the direct contact between the Ni and the magnet, the relevant magnetic field intensity has the highest attainable value (compare Figure 12S in the Supporting Information). This allows for maximizing the magnetic effect on the Ni spin polarization. The permanent magnet was a NdFeB B88X0 Grade N42 K&J Magnet, Inc., with a nickel coating: magnetic field at the surface is larger than 0.6 T (6353 Gauss).

2.3 XPS measurements

Spectra were taken at normal emission with a VG XR3 double anode X ray source delivering Mg Kα photons at 15 kV and 15 mA and with a CLAM2 VG hemispherical analyser driven at constant pass energy. Survey spectra were acquired with an analyser resolution of 2 eV, while elemental spectra where taken with a resolution of 0.5 eV.

3. Results

3.1 Chiral compound in solution: tartaric acid

CV curves recorded in the presence of the chiral organic compound in solution are shown together with the relevant base electrolyte (0.1 M KOH) CVs: figures 2 and 3. A quantitative assessment of the efficiency of the nickel oxidation process is carried out calculating the ratio between the current peaks in the presence of the chiral compound with respect to the current peak value of the relevant base electrolyte. Figure 2a shows CVs in a 0.5 mM solution of L-ta, the working electrode is Ni electrodeposited on the *north-pole* of a permanent magnet. The CV features one anodic (forward scan) current peak (P1a), at about 0.54 V (the 0.1 M KOH base electrolyte shows the anodic peak at 0.5 V). A rather broad cathodic peak (P1c, centred at 0.37 V) is present in the backward scan, for both the base electrolyte and the 0.5 mM L-ta acid solution. The peak in the forward scan is associated with the Ni(II) to Ni(III) oxidation process, *vide supra* [32,36,46,47].
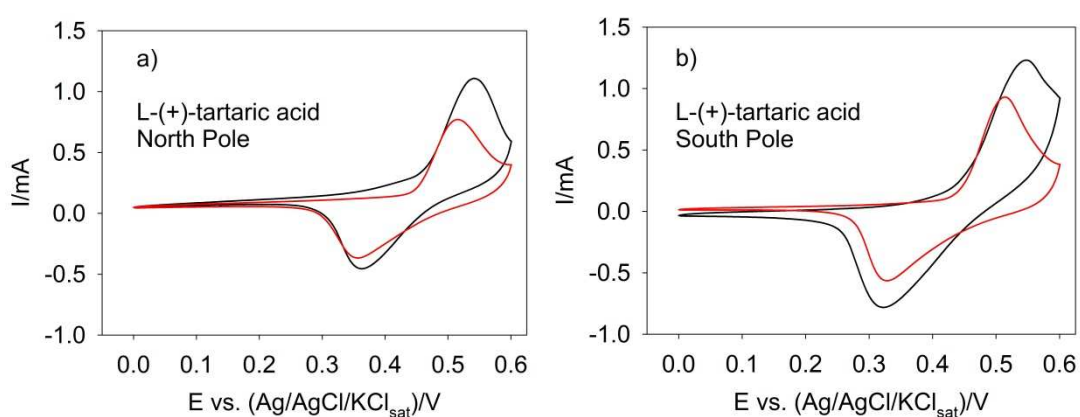

Figure 2. CV curves, the WE is Ni electrodeposited on magnet: a) **north pole** b) **south pole**. Red line: 0.1 M KOH. Black line: 0.5 mM L-ta acid in 0.1 M KOH aqueous solution. 50 mV/s scan rate, a Pt sheet is the CE, Ag/AgCl/KCl is the RE.

Notably, the area of the two (forward and backward) current peaks, which is related to the charge exchanged during the potential scan, is almost the same. This suggests that the chemistry of the redox processes underlying the current peaks in the CVs are of quasi-reversible nature. Figure 2b shows CVs recorded using a Ni surface, electrodeposited on the *south-pole* surface of a permanent magnet, in contact with a 0.5 mM solution of L-ta acid. Systematic differences are found in the potential values of the P1a and P1c redox peaks, as well as in the current peak ratio between the base electrolyte KOH solution and the L-ta solution. A larger potential peak to peak

separation, between the forward (oxidation) and backward (reduction) curves, is found in the case of the "south pole", compare CVs in Figures 2 a and b. This suggests a slightly better reversibility for the "north pole" working electrode. Focusing on the current peak values of the oxidation process a quantitative comparison, between the north and south pole nickel working electrodes, is carried out calculating the dimensionless quantity "anodic current ratio". The latter is calculated as the ratio between the anodic current of the oxidation peak on the same pole of the magnet, in the solutions containing the chiral compound and the base electrolyte: J_{Tart}/J_{KOH} where J_{Tart} is the P1a current for the TA solution and J_{KOH} is the P1a current for the base electrolyte. Thus, J_{Tart}/J_{KOH} is a quantitative measure of the ratio between the current of the solution containing the chiral compound and its "blank" (i.e. base electrolyte) solution. Such a simple index allows for the comparison of the electrochemical behaviour as a function of the magnet orientation Indeed, to unravel the role of the chiral compound in relation to the role of the magnet orientation (north or south, i.e. different spin "up" or "down" injection) in the oxidation process, we subtracted "anodic current ratio" values between the north and south pole electrodes:

$$sgn\left\{\left(\frac{J_{(Tart)}}{J_{(KOH)}}\right)_{(North)} - \left(\frac{J_{(Tart)}}{J_{(KOH)}}\right)_{(South)}\right\} \quad (5)$$

Where *sgn* is the sign function. Thus, the sign of relation (5) is positive if J_{Tart}/J_{KOH} ratio (from a measurement made on the north pole) is larger than the J_{Tart}/J_{KOH} (same operative conditions) on the south pole, a minus is obtained if the opposite holds. We obtained always a positive value, out of 18 measurements, indicating a "more favourable" process, i.e. a larger P1a current, on the north pole working electrode compared to the "south pole" one (numerical results are reported in Tables IVSI and VIISI, Supporting Information).

Figure 3a shows CVs of a 0.5 mM solution of D-ta, the working electrode is Ni obtained by electrodeposition on the ***north-pole*** surface of a permanent magnet. Please note that some of the features, here in particular the splitting of the backward reduction P1c peak in two sub peaks, depend on the initial state of the magnet surface, in particular affecting the reduction process (backward curve). In any case our procedure of determination of the "anodic current ratio" allows for taking into account, normalizing, such fluctuations in the CVs data which are related to the preparation of each new Ni surface. Anyhow, the areas (charge) for the oxidation process and for the

reduction process in Figure 3a, are about the same. Consistently with the results shown in Figure 2, the solution containing the chiral compound shows current always larger than the one recorded with only the base electrolyte (KOH), this both for the forward and backward scans.
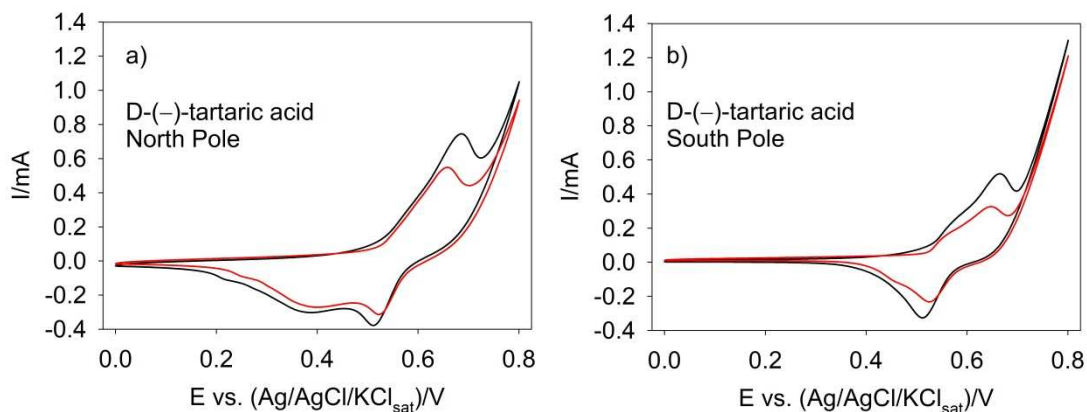

Figure 3. CV curves, the WE is Ni electrodeposited on magnet. Red line: 0.1 M KOH. Black line: 0.5 mM of D-(-)-tartaric acid in 0.1 M KOH aqueous solution. 50 mV/s potential scan rate, a Pt sheet is the CE, Ag/AgCl/KCl the RE. a) **north pole** b) **south pole**

As in the previous case of L-ta acid, "anodic current ratio" values are calculated for the 0.5 mM solution of D-ta. Remarkably, the difference between the "anodic current ratio", north-pole ratio minus south-pole ratio, is for the large majority of the cases (16 out of 18) negative, implying a larger increase in the anodic current ratio in the case of the south-pole of the magnet. This is at variance with the result obtained with the L-ta acid. Summarising, in the case of L-ta acid the north pole yields the larger increase in the anodic, P1a, ratio (with respect to the base electrolyte). Consistently, the opposite is found for the D-ta, in this case the nickel electrodeposited on the south pole leads to the larger anodic ratio.

3.2 Chiral ferromagnetic working electrode: Ni-LTA and Ni-DTA

This section shows results concerning the CFM electrode. Structure and composition of the CFM electrodes has been characterized via XPS spectroscopy measurements. Figure 4a compares survey spectra taken on a reference Ni-deposited electrode and co-deposited Ni-LTA electrodes, either on the south- or north-pole of a permanent magnet (Ni-LTA S and Ni-LTA N). The spectra are characterized by Ni2p, C1s and O1s well evident peaks, apart from residual contributions of Cl2p, due to the preparation of the electrodes. Resolved elemental structures are shown in Figure 4b-c.
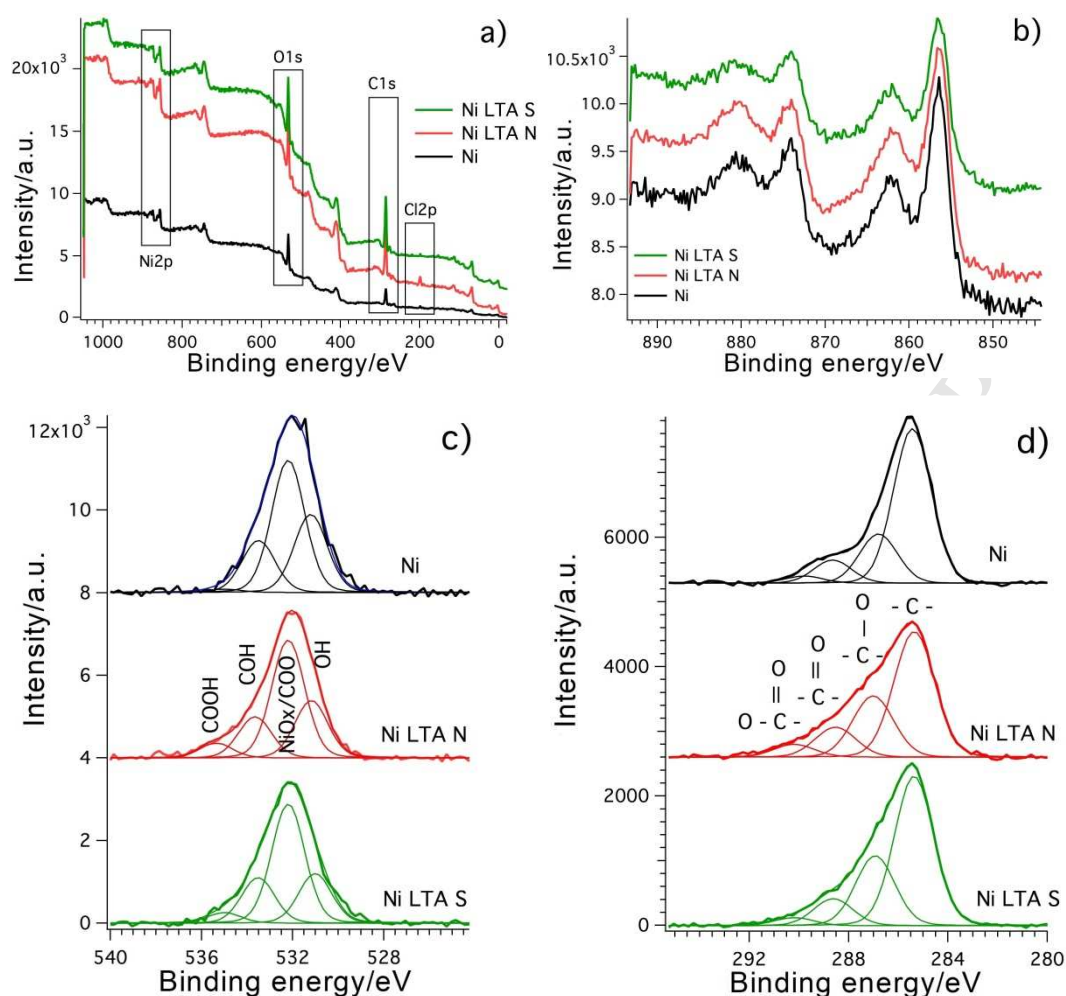
Figure 4. a) Survey spectra taken on a Ni-deposited electrode and co-deposited Ni-LTA electrodes with opposite directions of the magnetic field during growth (Ni LTA N and Ni LTA S). b) Resolved spectra of Ni 2p. c) Resolved spectra of O1s. d) Resolved spectra of C1s

In Figure 4b, the Ni2p spectra are shown. Ni appears oxidised, as expected for non-ideal samples not cleaned in ultra-high-vacuum and that passed from air before introduction in the vacuum vessel for analysis. The lineshape suggests a prevailing formation of hydroxides at the surface [48]. No sizable difference is present between the three samples, which indicates that neither LTA nor the magnetic field do alter the nature of the Ni film. O1s spectra, in Figure 4c show a broad structure, with maximum at about 532 eV for the three samples. In addition, LTA samples present a pronounced tail towards the high binding energy side. The spectra have been background subtracted and fitted with a set of Voigt curves [49]. OH groups contribute to the low binding energy side of the O1s structure. Other structures can be associated to contributions from O differently bonded to C and to Ni oxide [50]. In particular, the high binding energy tail is ascribed to COOH of tartaric acid, not present in the bare Ni sample. There's no

difference between samples prepared on the S and N poles of the magnet. C1s spectra are reported in Figure 4d. The most prominent peak is assigned to carbon from contaminants. It is interesting to note that the high binding energy tail, that can be associated to tartaric acid is present with equal contributions on both samples obtained on N and S poles, indicating no difference in concentration depending on the orientation of the magnetic field. Figure 5 a and b show CV curves of the CFM electrodes in 0.1 M KOH aqueous solution, base electrolyte. In this case the only chiral component in the system is the CFM electrode. Here the attention is focused on the electrochemical oxidation/reduction processes underlying the appearance of the oxidation, P1ox (centred at about +0.48 V), and reduction P1red (centred at about +0.39 V), found in the forward and backward CV curves, respectively. Please note that the current relevant to the oxidation and reduction peaks of the Ni(III)/Ni(II) redox process, Figure 5a, for the Ni-LTA south (solid line: 88 μA) is larger than that recorded on the north pole (dashed line: 69 μA). Remarkably, Figure 5b shows that the opposite is found for the Ni-DTA CFM working electrode: south 54 μA, north 64 μA. That is: upon flipping the magnetic field direction from north to south, the measured larger current swaps between the D-glu to the L-glu co-deposited nickel electrode. Figure 5c and 5d show CVs recorded in 0.1 M L-glu, or D-glu, in 0.1 M KOH aqueous solution base electrolyte. The WE is the chiral ferromagnetic imprinted working electrode: Ni-LTA and Ni-DTA. For the sake of clarity only the forward scan is shown.
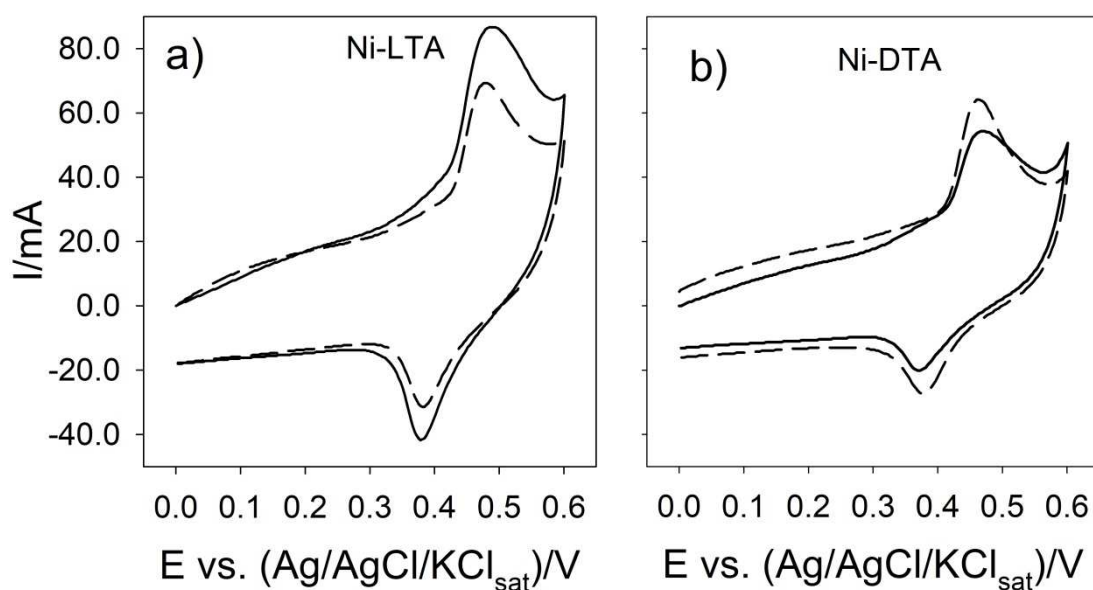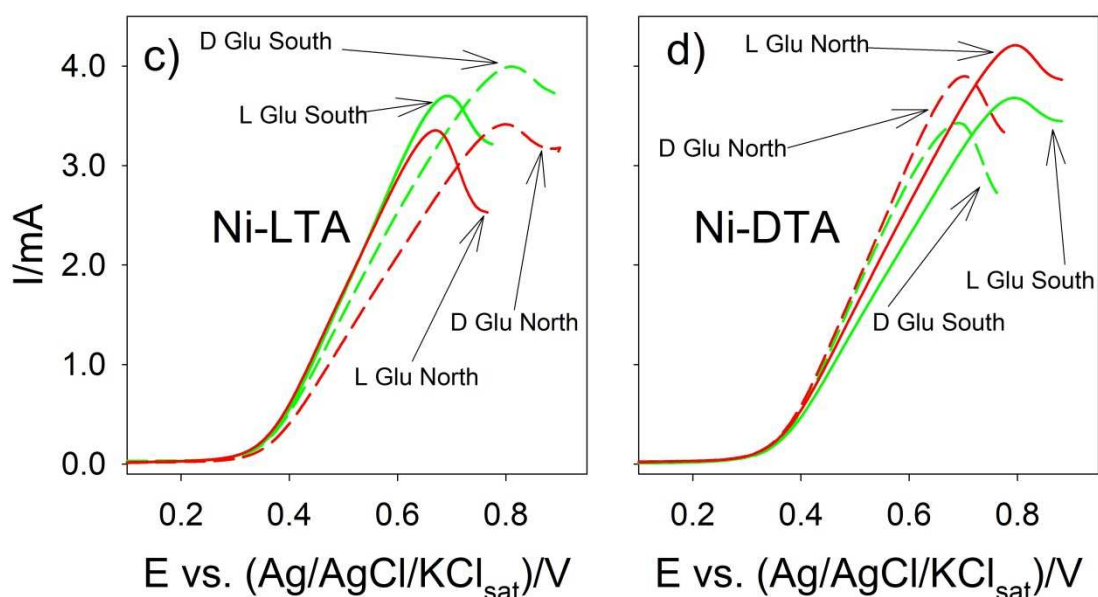
Figure 5. CV curves in 0.1 M KOH aqueous solution: a) Ni co-deposited with L-ta acid WE b) Ni co-deposited with D-ta WE. Solid line: electrodeposition on the south pole. Dashed line: electrodeposition on the north pole. c) Ni-LTA WE, north and south, in enantiopure solution of 0.1 M L-glu or D-glu. d) Ni-LDA WE, north and south, in enantiopure solution of 0.1 M L-glu or D-glu. Solid red line: L-glu on north. Dashed red line: D-(+)-glucose on north. Solid green line: L-glu on south. Dashed green line: D-(+)-glucose on south.

Figure 5c shows that the oxidation of L-glu is easier, i.e. the peak potential is less positive (about +0.69 V), with respect to the D-glu one (+0.81 V). The opposite is found when the Ni-DTA electrode is used: the oxidation of D-glu is easier, i.e. the peak potential is less positive (about +0.68 V), with respect the L-glu one (+0.79 V). Also the peak currents show a regular symmetric pattern as a function of the CFM and of the north and south poles. Remarkably, the CVs of the enantiomers are clearly discriminated, demonstrating a substantial ability of the Ni-LTA electrode, in the process of enantio-recognition. The difference in the oxidation peak is about 0.1 V, in particular, *i)* Ni-LTA: the potential peak difference between D-glu and L-glu is 0.12 V *ii)* Ni-DTA: the peak potential difference between L-glu and D-glu is 0.11 V[1]. Note that, the glucose CVs do not show any of the peak related to the Ni oxidation/reduction processes. This result can be due to glucose adsorption on the electrode surface leading to inhibition of the nickel oxidation, at increasing the potential glucose is oxidized to gluconolactone, reaction (6), with a complex process involving a large number of adsorbed intermediate species [37,38,51–54]:

---

[1] A crude estimation of the error affecting the whole procedure of electrodeposition and CV measurement on Ni CFM electrodes shows a 3% maximum variation (CVs repeated at least five times, in two different laboratories). Which means for the potential differences: 0.12 ± 0.0036 V and 0.12 ± 0.0033 V,

$$NiOOH + glucose \rightarrow Ni(OH)_2 + gluconolactone + 2e^- \tag{6}$$
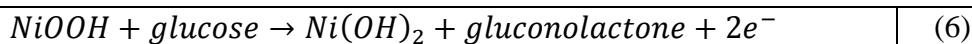
4. Discussion

The idea that chiral compounds present in bulk system are able to "induce" enantio-selectivity, or generate local spatial chirality, effects [14,15] is implemented within the spin-dependent electrochemistry approach following two different strategies:

a) Chirality effects induced by the presence of a chiral compound in bulk solution: in the case of the tartaric acid, D or L enantiomer, the current recorded in the presence of the bulk chiral compound, black line, is systematically larger than that of the base electrolyte, red curve, compare Figures 2 and 3. In this case the effect of the presence of the chiral compound in bulk solution has been investigated by comparing the oxidation peak current values as a function of the magnet orientation (north vs. south). Data relevant to the systematic analysis of the experimental results are available in the Supporting Information, Table ISI to Table IXSI. In particular, the sign found in column titled "sgn(J_{ratio} North $-$ J_{ratio} South)" (Table IVSI and Table VIISI in the Supporting Information) gives the indication of the most efficient combination: in terms of the larger variation in peak current induced by presence of the tartaric acid (with respect to the "blank solution[2]". Remarkably, the L-ta acid north is found more effective than L-ta acid south, and in a consistent way the D-(-)-tartaric acid south combination is found more effective than the D-(-)-tartaric acid north. Table VIIISI and Table IXSI report the percentage of spin polarization current, as obtained using equation 7:

$$\frac{\left(\frac{J_{(Tart)}}{J_{(KOH)}}\right)_{(North)} - \left(\frac{J_{(Tart)}}{J_{(KOH)}}\right)_{(South)}}{\left(\frac{J_{(Tart)}}{J_{(KOH)}}\right)_{(North)} + \left(\frac{J_{(Tart)}}{J_{(KOH)}}\right)_{(South)}} \times 100 = SP\% \tag{7}$$

b) The new concept, here presented, of the hybrid chiral ferromagnetic electrode supported on a magnet, proved to be an efficient system for enantio-selective discrimination, and an efficient spin-valve as well. The spin valve behavior is proved by the CVs recorded for the achiral Ni(III)/Ni(II) redox process as a function only of the magnetic field direction (i.e. north vs. south). This result is only due to the interaction of the chiral nature of the CFM with the magnetic field orientation. The enantio-selectivity is substantiated by the consistent discrimination in oxidation peak potential found in the CVs recorded in solution of the glucose enantiomer: a potential separation of 0.1 V is found on the glucose oxidation potential when comparing the two enantiomers CVs.

---

[2] 0.1 M KOH base electrolyte solution

The latter potential difference is a function of both the chiral nature of the CFM and as a function of the magnetic field orientation. In tight analogy to the results shown when chiral surfaces are considered [7–10,55]. Note that, spin-polarization can affect the first stage of the glucose oxidation: the first elementary step in the oxidation reaction is the adsorption of glucose upon dehydrogenation, followed by oxidation to gluconate [37,38,51–54]:

$$glucose_{bulk} + OH^-_{bulk} \rightarrow (dehydrogenated\ glucose)_{adsorbed} + H_2O + e^- \quad (8)$$
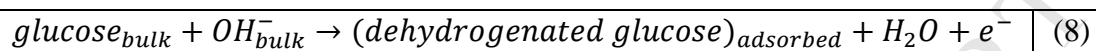
Indeed, chiral-induced spin-selectivity (CISS) effects are known to affect adsorption and enantio-selectivity through polarization effect [24,56]. This appears the key to rationalize the discriminating ability of the CFM, Ni-LTA and Ni-DTA, north vs. south electrode. This result can be addressed as an example of chemical reactivity driven by the CISS effect.

5. Conclusion

In this work we exploit the idea that the presence of chiral compounds is able to generate local "spatial chirality effects", or in other words to "induce" enantio-selectivity [4,14,15]. Our innovative idea is to combine the "induced spatial chirality effect" with the CISS effect, the implementation of such a concept is pursued in two different ways.

a) Presence of a chiral compound in bulk solution coupled with a standard spin-dependent electrochemistry set-up. The major variation concerns the nickel ferromagnetic electrode, which is directly deposited on the magnet. An average of 4 % spin polarization, SP, is obtained (average obtained by the SP values of a rather large number of experiments). Such a value is definitively less than the 15 % to 20 % SP range obtained in the case of well-ordered chiral monolayers directly adsorbed on top of ferromagnetic electrode surface [16,17,57,58]. The advantage is that using bulk compounds the preparation of the chiral system is by far easier.

b) A completely new concept is proposed: the chiral compound is co-deposited (embedded) within the bulk ferromagnetic electrode. Ni is chiral imprinted by co-deposition with the tartaric acid. In this case the "CFM electrode"/magnet orientation by itself is expected to couple the spin injection (alpha/beta DOS manipulation obtained by applying the magnetic field) with the CISS. That is a combined, magnetic field/chiral, spin selective injecting system. Indeed, the intrinsic spin transport characteristic of the CFM is proved by the CVs recorded in KOH solution, where only the achiral

Ni(III)/Ni(II) redox process is active. In this case the difference in current observed upon flipping the magnetic field, north vs. south, is certainly due to the high spin-selective transport properties of the Ni CFM electrode: SP = 11%. What is more, a systematic difference is found in the CVs measured in the glucose solution upon flipping the magnetic field direction, north and south poles of the Ni-LTA electrode (results confirmed by the complementary electrochemical behaviour observed with the Ni-DTA CFM electrode). A clear-cut discrimination is obtained in the glucose oxidation peak potential: the difference in the D-glu vs. L-glu oxidation peak potential, as a function of the magnetic field and of the nature of chiral imprinting of the CFM, is larger than 0.1 V. This last impressive result gives further impulse to the scientific research concerning the role of spin in the enantio-recognition process [15,30,56].

References

[1]   R. Naaman, D.N. Beratan, D. Waldeck, eds., Electronic and Magnetic Properties of Chiral Molecules and Supramolecular Architectures, Springer-Verlag, Berlin Heidelberg, 2011. //www.springer.com/la/book/9783642181030 (accessed May 5, 2018).

[2]   D.G. Blackmond, The origin of biological homochirality, Philos. Trans. R. Soc. B Biol. Sci. 366 (2011) 2878–2884. doi:10.1098/rstb.2011.0130.

[3]   M. Stich, J.M. Ribó, D.G. Blackmond, D. Hochberg, Necessary conditions for the emergence of homochirality via autocatalytic self-replication, J. Chem. Phys. 145 (2016) 074111. doi:10.1063/1.4961021.

[4]   F. Sannicolò, S. Arnaboldi, T. Benincori, V. Bonometti, R. Cirilli, L. Dunsch, W. Kutner, G. Longhi, P.R. Mussini, M. Panigati, M. Pierini, S. Rizzo, Potential-Driven Chirality Manifestations and Impressive Enantioselectivity by Inherently Chiral Electroactive Organic Films, Angew. Chem. Int. Ed. 53 (2014) 2623–2627. doi:10.1002/anie.201309585.

[5]   F. Sannicolò, P.R. Mussini, T. Benincori, R. Martinazzo, S. Arnaboldi, G. Appoloni, M. Panigati, E. Quartapelle Procopio, V. Marino, R. Cirilli, S. Casolo, W. Kutner, K. Noworyta, A. Pietrzyk-Le, Z. Iskierko, K. Bartold, Inherently Chiral Spider-Like Oligothiophenes, Chem. – Eur. J. 22 (2016) 10839–10847. doi:10.1002/chem.201504899.

[6]   F. Tassinari, S.P. Mathew, C. Fontanesi, L. Schenetti, R. Naaman, Electric-Field-Driven Alignment of Chiral Conductive Polymer Thin Films, Langmuir. 30 (2014) 4838–4843. doi:10.1021/la500657e.

[7]   J.A. Switzer, H.M. Kothari, P. Poizot, S. Nakanishi, E.W. Bohannan, Enantiospecific electrodeposition of a chiral catalyst, Nature. 425 (2003) 490–493. doi:10.1038/nature01990.

[8]   E.W. Bohannan, H.M. Kothari, I.M. Nicic, J.A. Switzer, Enantiospecific Electrodeposition of Chiral CuO Films on Single-Crystal Cu(111), J. Am. Chem. Soc. 126 (2004) 488–489. doi:10.1021/ja039422+.

[9]   H.M. Kothari, E.A. Kulp, S. Boonsalee, M.P. Nikiforov, E.W. Bohannan, P. Poizot, S. Nakanishi, J.A. Switzer, Enantiospecific Electrodeposition of Chiral CuO Films from Copper(II) Complexes of Tartaric and Amino Acids on Single-Crystal Au(001), Chem. Mater. 16 (2004) 4232–4244. doi:10.1021/cm048939x.

[10] C. Wattanakit, Y.B.S. Côme, V. Lapeyre, P.A. Bopp, M. Heim, S. Yadnum, S. Nokbin, C. Warakulwit, J. Limtrakul, A. Kuhn, Enantioselective recognition at mesoporous chiral metal surfaces, Nat. Commun. 5 (2014) ncomms4325. doi:10.1038/ncomms4325.

[11] I. Mogi, K. Watanabe, Chirality of Magnetoelectropolymerized Polyaniline Electrodes, Jpn. J. Appl. Phys. 44 (2005) L199–L201. doi:10.7567/JJAP.44.L199.

[12] I. Mogi, K. Watanabe, Chirality of magneto-electrodeposited metal film electrodes, Sci. Technol. Adv. Mater. 9 (2008) 024210. doi:10.1088/1468-6996/9/2/024210.

[13] I. Mogi, K. Watanabe, Chiral Recognition of Amino Acids by Magnetoelectrodeposited Cu Film Electrodes, Int. J. Electrochem. 2011 (2011). doi:10.4061/2011/239637.

[14] S. Arnaboldi, R. Cirilli, A. Forni, A. Gennaro, A.A. Isse, V. Mihali, P.R. Mussini, M. Pierini, S. Rizzo, F. Sannicolò, Electrochemistry and Chirality in Bibenzimidazole

Systems, Electrochimica Acta. 179 (2015) 250–262. doi:10.1016/j.electacta.2015.03.177.

[15] S. Rizzo, S. Arnaboldi, V. Mihali, R. Cirilli, A. Forni, A. Gennaro, A.A. Isse, M. Pierini, P.R. Mussini, F. Sannicolò, "Inherently Chiral" Ionic-Liquid Media: Effective Chiral Electroanalysis on Achiral Electrodes, Angew. Chem. Int. Ed. 56 (2017) 2079–2082. doi:10.1002/anie.201607344.

[16] D. Mishra, T.Z. Markus, R. Naaman, M. Kettner, B. Göhler, H. Zacharias, N. Friedman, M. Sheves, C. Fontanesi, Spin-dependent electron transmission through bacteriorhodopsin embedded in purple membrane, Proc. Natl. Acad. Sci. 110 (2013) 14872–14876. doi:10.1073/pnas.1311493110.

[17] P.C. Mondal, N. Kantor-Uriel, S.P. Mathew, F. Tassinari, C. Fontanesi, R. Naaman, Chiral Conductive Polymers as Spin Filters, Adv. Mater. 27 (2015) 1924–1927. doi:10.1002/adma.201405249.

[18] P.C. Mondal, C. Fontanesi, D.H. Waldeck, R. Naaman, Spin-Dependent Transport through Chiral Molecules Studied by Spin-Dependent Electrochemistry, Acc. Chem. Res. (2016). doi:10.1021/acs.accounts.6b00446.

[19] C. Fontanesi, Spin-dependent electrochemistry: A novel paradigm, Curr. Opin. Electrochem. 7 (2018) 36–41. doi:10.1016/j.coelec.2017.09.028.

[20] K. Ray, S.P. Ananthavel, D.H. Waldeck, R. Naaman, Asymmetric Scattering of Polarized Electrons by Organized Organic Films of Chiral Molecules, Science. 283 (1999) 814–816. doi:10.1126/science.283.5403.814.

[21] R. Naaman, D.H. Waldeck, Spintronics and Chirality: Spin Selectivity in Electron Transport Through Chiral Molecules, Annu. Rev. Phys. Chem. 66 (2015) 263–281. doi:10.1146/annurev-physchem-040214-121554.

[22] I. Carmeli, K.S. Kumar, O. Heifler, C. Carmeli, R. Naaman, Spin Selectivity in Electron Transfer in Photosystem I, Angew. Chem. Int. Ed. 53 (2014) 8953–8958. doi:10.1002/anie.201404382.

[23] O.B. Dor, S. Yochelis, S.P. Mathew, R. Naaman, Y. Paltiel, A chiral-based magnetic memory device without a permanent magnet, Nat. Commun. 4 (2013) ncomms3256. doi:10.1038/ncomms3256.

[24] O. Ben Dor, S. Yochelis, A. Radko, K. Vankayala, E. Capua, A. Capua, S.-H. Yang, L.T. Baczewski, S.S.P. Parkin, R. Naaman, Y. Paltiel, Magnetization switching in ferromagnets by adsorbed chiral molecules without current or external magnetic field, Nat. Commun. 8 (2017) 14567. doi:10.1038/ncomms14567.

[25] W. Mtangi, V. Kiran, C. Fontanesi, R. Naaman, Role of the Electron Spin Polarization in Water Splitting, J. Phys. Chem. Lett. 6 (2015) 4916–4922. doi:10.1021/acs.jpclett.5b02419.

[26] W. Mtangi, F. Tassinari, K. Vankayala, A. Vargas Jentzsch, B. Adelizzi, A.R.A. Palmans, C. Fontanesi, E.W. Meijer, R. Naaman, Control of Electrons' Spin Eliminates Hydrogen Peroxide Formation During Water Splitting, J. Am. Chem. Soc. 139 (2017) 2794–2798. doi:10.1021/jacs.6b12971.

[27] C. Fontanesi, R. Naaman, W. Mtangi, Water splitting method and system, WO 2016056011 A1, 2016.

[28] X. Liang, J. Liu, D. Zeng, C. Li, S. Chen, H. Li, Hydrogen generation promoted by photocatalytic oxidation of ascorbate and glucose at a cadmium sulfide electrode, Electrochimica Acta. 198 (2016) 40–48. doi:10.1016/j.electacta.2016.03.023.

[29] R. Naaman, D.H. Waldeck, Chiral-Induced Spin Selectivity Effect, J. Phys. Chem. Lett. 3 (2012) 2178–2187. doi:10.1021/jz300793y.

[30] A. Kumar, E. Capua, K. Vankayala, C. Fontanesi, R. Naaman, Magnetless Device for Conducting Three-Dimensional Spin-Specific Electrochemistry, Angew. Chem. Int. Ed. 56 (2017) 14587–14590. doi:10.1002/anie.201708829.

[31] G. Kresse, J. Furthmüller, Efficient iterative schemes for \textit{ab initio} total-energy calculations using a plane-wave basis set, Phys. Rev. B. 54 (1996) 11169–11186. doi:10.1103/PhysRevB.54.11169.

[32] M.R. Barbosa, Comparative Potentiodynamic Study of Nickel in Still and Stirred Sulfuric Acid-Potassium Sulfate Solutions in the 0.4–5.7 pH Range, J. Electrochem. Soc. 135 (1988) 1077. doi:10.1149/1.2095878.

[33] Z. Mekhalif, F. Laffineur, N. Couturier, J. Delhalle, Elaboration of Self-Assembled Monolayers of n-Alkanethiols on Nickel Polycrystalline Substrates: Time, Concentration, and Solvent Effects, Langmuir. 19 (2003) 637–645. doi:10.1021/la020332c.

[34] F. Loglio, M. Innocenti, A. Jarek, S. Caporali, I. Pasquini, M.L. Foresti, Nickel sulfur thin films deposited by ECALE: Electrochemical, XPS and AFM characterization, J. Electroanal. Chem. 638 (2010) 15–20. doi:10.1016/j.jelechem.2009.10.027.

[35] S. Rajalingam, S. Devillers, J. Dehalle, Z. Mekhalif, A two step process to form organothiol self-assembled monolayers on nickel surfaces, Thin Solid Films. 522 (2012) 247–253. doi:10.1016/j.tsf.2012.08.036.

[36] J. Qiao, S. Tang, Y. Tian, S. Shuang, C. Dong, M.M.F. Choi, Electro-catalytic oxidation of methane at multi-walled carbon nanotubes-Nafion/nickel hydroxide modified nickel electrode, Sens. Actuators B Chem. 138 (2009) 402–407. doi:10.1016/j.snb.2009.02.065.

[37] C. Wang, L. Yin, L. Zhang, R. Gao, Ti/TiO2 Nanotube Array/Ni Composite Electrodes for Nonenzymatic Amperometric Glucose Sensing, J. Phys. Chem. C. 114 (2010) 4408–4413. doi:10.1021/jp912232p.

[38] Y. Mu, D. Jia, Y. He, Y. Miao, H.-L. Wu, Nano nickel oxide modified non-enzymatic glucose sensors with enhanced sensitivity through an electrochemical process strategy at high potential, Biosens. Bioelectron. 26 (2011) 2948–2952. doi:10.1016/j.bios.2010.11.042.

[39] W. Yi, D. Yang, H. Chen, P. Liu, J. Tan, H. Li, A highly sensitive nonenzymatic glucose sensor based on nickel oxide–carbon nanotube hybrid nanobelts, J. Solid State Electrochem. 18 (2014) 899–908. doi:10.1007/s10008-013-2329-3.

[40] C. Fontanesi, F. Tassinari, F. Parenti, H. Cohen, P.C. Mondal, V. Kiran, A. Giglia, L. Pasquali, R. Naaman, New One-Step Thiol Functionalization Procedure for Ni by Self-Assembled Monolayers, Langmuir. 31 (2015) 3546–3552. doi:10.1021/acs.langmuir.5b00177.

[41] M.-S. Wu, F.-Y. Chen, Y.-H. Lai, Y.-J. Sie, Electrocatalytic oxidation of urea in alkaline solution using nickel/nickel oxide nanoparticles derived from nickel-organic framework, Electrochimica Acta. 258 (2017) 167–174. doi:10.1016/j.electacta.2017.10.113.

[42] S.K. Yadav, J. Singh, V.V. Agrawal, B.D. Malhotra, Nanostructured nickel oxide film for application to fish freshness biosensor, Appl. Phys. Lett. 101 (2012) 023703. doi:10.1063/1.4736578.

[43] D.S. Hall, D.J. Lockwood, C. Bock, B.R. MacDougall, Nickel hydroxides and related materials: a review of their structures, synthesis and properties, Proc R Soc A. 471 (2015) 20140792. doi:10.1098/rspa.2014.0792.

[44] W. Visscher, E. Barendrecht, Absorption of hydrogen in reduced nickel oxide, J. Appl. Electrochem. 10 (1980) 269–274. doi:10.1007/BF00726096.

[45] A. Seghiouer, J. Chevalet, A. Barhoun, F. Lantelme, Electrochemical oxidation of nickel in alkaline solutions: a voltammetric study and modelling, J. Electroanal. Chem. 442 (1998) 113–123. doi:10.1016/S0022-0728(97)00498-1.

[46] R.S.S. Guzmán, J.R. Vilche, A.J. Arvía, Rate Processes Related to the Hydrated Nickel Hydroxide Electrode in Alkaline Solutions, J. Electrochem. Soc. 125 (1978) 1578–1587. doi:10.1149/1.2131247.

[47] A.A. El-Shafei, Electrocatalytic oxidation of methanol at a nickel hydroxide/glassy carbon modified electrode in alkaline medium, J. Electroanal. Chem. 471 (1999) 89–95. doi:10.1016/S0022-0728(99)00235-1.

[48] N.S. McIntyre, M.G. Cook, X-ray photoelectron studies on some oxides and hydroxides of cobalt, nickel, and copper, Anal. Chem. 47 (1975) 2208–2213. doi:10.1021/ac60363a034.

[49] C. Jiang, B. Zhao, J. Cheng, J. Li, H. Zhang, Z. Tang, J. Yang, Hydrothermal synthesis of Ni(OH)2 nanoflakes on 3D graphene foam for high-performance supercapacitors, Electrochimica Acta. 173 (2015) 399–407. doi:10.1016/j.electacta.2015.05.081.

[50] S. Baldanza, J. Ardini, A. Giglia, G. Held, Stereochemistry and thermal stability of tartaric acid on the intrinsically chiral Cu{531} surface, Surf. Sci. 643 (2016) 108–116. doi:10.1016/j.susc.2015.08.021.

[51] L.-M. Lu, L. Zhang, F.-L. Qu, H.-X. Lu, X.-B. Zhang, Z.-S. Wu, S.-Y. Huan, Q.-A. Wang, G.-L. Shen, R.-Q. Yu, A nano-Ni based ultrasensitive nonenzymatic electrochemical sensor for glucose: Enhancing sensitivity through a nanowire array strategy, Biosens. Bioelectron. 25 (2009) 218–223. doi:10.1016/j.bios.2009.06.041.

[52] M. Pasta, F. La Mantia, Y. Cui, Mechanism of glucose electrochemical oxidation on gold surface, Electrochimica Acta. 55 (2010) 5561–5568. doi:10.1016/j.electacta.2010.04.069.

[53] G. Ma, M. Yang, C. Li, H. Tan, L. Deng, S. Xie, F. Xu, L. Wang, Y. Song, Preparation of spinel nickel-cobalt oxide nanowrinkles/reduced graphene oxide hybrid for nonenzymatic glucose detection at physiological level, Electrochimica Acta. 220 (2016) 545–553. doi:10.1016/j.electacta.2016.10.163.

[54] S. Karra, M. Wooten, W. Griffith, W. Gorski, Morphology of Gold Nanoparticles and Electrocatalysis of Glucose Oxidation, Electrochimica Acta. 218 (2016) 8–14. doi:10.1016/j.electacta.2016.09.097.

[55] R. Widmer, F.-J. Haug, P. Ruffieux, O. Gröning, M. Bielmann, P. Gröning, R. Fasel, Surface Chirality of CuO Thin Films, J. Am. Chem. Soc. 128 (2006) 14103–14108. doi:10.1021/ja0640703.

[56] A. Kumar, E. Capua, M.K. Kesharwani, J.M.L. Martin, E. Sitbon, D.H. Waldeck, R. Naaman, Chirality-induced spin polarization places symmetry constraints on biomolecular interactions, Proc. Natl. Acad. Sci. 114 (2017) 2474–2478. doi:10.1073/pnas.1611467114.

[57] M. Kettner, B. Göhler, H. Zacharias, D. Mishra, V. Kiran, R. Naaman, C. Fontanesi, D.H. Waldeck, S. Sęk, J. Pawłowski, J. Juhaniewicz, Spin Filtering in Electron Transport Through Chiral Oligopeptides, J. Phys. Chem. C. 119 (2015) 14542–14547. doi:10.1021/jp509974z.

[58] P.C. Mondal, C. Fontanesi, D.H. Waldeck, R. Naaman, Field and Chirality Effects on Electrochemical Charge Transfer Rates: Spin Dependent Electrochemistry, ACS Nano. (2015). doi:10.1021/acsnano.5b00832.